Draft version August 15, 2022
Typeset using LaTeX **twocolumn** style in AASTeX631

Translational Tomography with the Wide-field Imager for Parker Solar Probe (WISPR) I: Theoretical basis and initial modeling

M. N. Kenny,[1] C. E. DeForest,[2] M. J. West,[2] and P. C. Liewer[3]

[1] *University of Colorado, Boulder*
2000 Colorado Ave, Boulder, CO 80305, USA
[2] *Southwest Research Institute*
1050 Walnut St 300, Boulder, CO 80302, USA
[3] *Jet Propulsion Laboratory*
California Institute of Technology, Pasadena, CA 91109, USA

ABSTRACT

In the first of a planned sequence of articles, we present a simple method for reconstructing radial density structures of the solar corona in the vicinity of the Parker Solar Probe (PSP) near and during perihelion passes. We describe how we model the apparent kinematics of stationary K-Corona striae from PSP-WISPR's viewpoint using a simple two-parameter model, form a partial basis of the data space that is a WISPR image sequence, and change the basis from image coordinates to 'tomographic coordinates' in order to determine the parameters of such features. We apply the method to a simple three-dimensional (3D) model of a WISPR coronal flythrough, demonstrate the ways that it succeeds and fails, and discuss possible improvements to the sensitivity and applicability of the our model for real WISPR data.

Keywords: Parker Solar Probe, WISPR, tomography, corona, solar wind, radial solar wind features

1. INTRODUCTION

1.1. *The Corona, the Solar Wind, and Imaging of the Heliosphere*

The outermost region of the solar atmosphere, the solar corona, is characterized by low density – $\sim 10^6$ cm^{-3} in the upper corona at a height of one solar radius to 10^9 cm^{-3} at the base in quiet regions – and high temperatures – millions of degrees Kelvin (Aschwanden 2006). In the magnetically dominated (low-β) regime of the low corona, charged particles follow the magnetic field, while in the high corona and solar wind, the magnetic field follows the plasma. Where the plasma-β is low, the magnetic pressure dominates thermal (i.e. static) pressure; however, the dynamic pressure overtakes the magnetic pressure, thus structuring the corona radially. Magnetic structures and magnetically driven events originating in the corona play a major role in connecting the Sun to the greater the solar system. Observing long-lived, large-scale radial features, or striae, in the corona provides windows into the underlying magnetic processes and solar wind formation and acceleration mechanisms. (Golub & Pasachoff 2010)

Until Bernard Lyot's invention of the coronagraph in 1930, total solar eclipses provided the only opportunities to observe faint tenuous structures in the corona in visible light wavelengths. However, with both ground-based and space-based coronagraphs and heliospheric imagers in operation, we can now continuously observe coronal features. Coronagraphs and heliospheric imagers alike detect broadband visible light Thomson-scattered off free electrons in the plasma that the instrument observes (DeForest et al. 2011). Space-borne coronagraphs began operating routinely in the 1970s, which improved streamer observation capabilities (Decraemer et al. 2019). In 1995, the Solar and Heliospheric Observatory (SOHO) was launched with a dozen on-board instruments, including the Large Angle and Spectrometric COronagraph (LASCO) (Brueckner et al. 1995). LASCO coronagraph data enabled the development of many electron density distribution models with its high resolution total brightness observations; see Decrae-

Corresponding author: M. N. Kenny
megan.kenny@colorado.edu

mer et al. (2019) and references therein. Furthermore, LASCO C2/C3 data have validated and supplemented a myriad of other observations and models, such as white-light eclipse observations of small-scale streamer structures e.g. Koutchmy (1994); magnetic field extrapolations to the corona from photospheric magnetograms, e.g. Sasso et al. (2019); and coronal magnetic field extrapolations from potential field source surface (PFSS) models, e.g. Liewer et al. (2001).

The Solar Mass Ejection Imager (SMEI) (Eyles et al. 2003) and the Sun Earth Connection Coronal and Heliospheric Investigation (SECCHI) package onboard the twin STEREO spacecraft (Howard et al. 2008) have constituted major instrumental advancements which have thereby generated major scientific progress in coronal research. However, it wasn't until the launch of Parker Solar Probe Fox et al. (2016) that a heliospheric imager – WISPR – entered the inner heliosphere.

As an imager on-board PSP, WISPR sees heliospheric structures from within the inner heliosphere. Its novel viewpoint provides novel science opportunities. For example, we can reconstruct local coronal structure using image sequences from WISPR. As opposed to the traditional tomographic approach by which one uses rotation to accrue multiple viewpoints, we use WISPR's translational motion past and through coronal features to provide multiple viewing angles.

Reconstructing structure from multiple viewpoints is the domain of tomography, which is a particular application of the very broad topic of inverse theory. As Menke describes in *Geophysical Data Analysis*, "inverse theory is an organized set of mathematical techniques for reducing data to obtain knowledge about the physical world on the basis of inferences drawn from observations" (2018). In other words, we start with a dataset and a general principle, theory, or model with the goal of determining the underlying physics (Menke 2018). As opposed to forward problems, wherein one begins with a theory and seeks to predict, with a hypothesis or model, what the data will show, inverse problems do the opposite.

The specific inverse problem of interest, tomography, involves reconstructing an N-dimensional image of a system using (N-1)-dimensional line-of-sight measurements through the system. Typical tomographic applications include rotating the subject to provide a complete set of angular views, or in the case of the Sun, allowing the subject's natural rotation to provide such viewpoints; these applications use an orthogonal sine-wave basis to reconstruct the system. The first recorded coronal tomography study involved reconstructing the 3D electron density distribution of the inner solar corona as a function of radial distance, latitude, and longitude from K-coronameter polarization brightness measurements (Altschuler 1979). This method was later dubbed solar rotational tomography (SRT). It is limited by coronal evolution during a solar revolution but retains the mathematical structure of more conventional tomographic inversion from a complete set of viewing angles over a full circle. Other seminal studies have included reconstruction of emissivities in the solar corona for neutral hydrogen Lyman α lines using the Ultraviolet Coronagraph Spectrometer (UVCS) onboard SOHO (Panasyuk 1999). Altschuler & Perry's technique of solar rotational tomography to solve for 3D electron density distributions has been a major area of research for the last five decades, most recently explored by Frazin (2000), Frazin & Janzen (2002), and Jackson et al. (2011).

A novel application of SRT investigated the potential of synthetic WISPR image sequences in carrying out tomographic reconstructions of the electron density (Vásquez et al. 2019). They synthesized total brightness images using the precise orbital information of PSP from a static 3D magneto-hydrodynamic (MHD) model of the corona and compared their reconstruction results with the model (Vásquez et al. 2019). This study demonstrated that WISPR, at least in principle, has the capability to carry out tomographic reconstructions of the corona. Vourlidas et al. (2016) described how WISPR's rapidly changing FoV would enable detailed tomographic reconstructions of the large and small-scale structure of the background corona; thus, WISPR provides both broad and detailed context for interpreting the in-situ PSP measurements.

Unlike SRT techniques and the recent forward modeling of WISPR images by Vásquez et al. (2019), our novel method of tomography contains an incomplete set of view angles and a different path through the plasma. The reduced set of viewing angles and nearly-linear translational motion through the corona has disadvantages (e.g. an incomplete basis) as well as advantages (e.g. capacity to look for smaller structure).

In Section 2 we describe the details of Parker Solar Probe and its imager WISPR. In Section 3 we step through the process by which we drew up an analytic model for apparent streamer motion in the WISPR FoV and tested this model on a simulated flythrough dataset. In Section 4, we show and analyze the results of the inversion, and in Sections 5 and 6 we discuss the meaning and implications of the results, draw conclusions, and indicate next steps. We motivate the use of translational tomography and introduce the reader to the method. We follow an iterative approach: In this first paper, we

describe linear translation as a means to develop a tomogram. In subsequent papers, we will generalize to geometries reflective of the actual PSP orbit.

2. INSTRUMENTATION

Parker Solar Probe (PSP) is a NASA heliophysics mission that launched in August of 2018 to investigate the inner heliospheric plasma by flying in elliptical heliocentric orbits (Fox et al. 2016). With decreasing orbital radius over the spacecraft's nominal 24 orbits, PSP probes ever-closer plasma to our local star. In the first orbit, PSP's perihelion was 35 $R_\odot$, and the final three perihelia of the primary mission will get down to $9.86 R_\odot$.

Onboard the spacecraft sit four instrument suites with distinct scientific goals; of these four instrument suites, three measure plasma *in situ* and one images coronal structures in visible light. We use data from the imager: the *Wide-field Imager for Parker Solar Probe* (WISPR) which captures continuous, synoptic images of coronal features in visible light(Vourlidas et al. 2016). An inner (WISPR-I) and outer (WISPR-O) telescope, both with squares fields of view (FoV) collectively span a 95° extent off the limb of the solar disk. WISPR-I spans 13.5°-53.5° and has a passband of 490-740 nm, and WISPR-O spans 50.5°-108.5° and has a passband of 475-725 nm (with a 3° overlap) (Vourlidas et al. 2016). As PSP's distance changes, so do the size scales in the fixed FoV: E.g. the WISPR-I FoV cutoff at 13.5° corresponds to a heliocentric distance of 2.3 $R_\odot$ at 9.86 $R_\odot$ (Vourlidas et al. 2016).

The brightest feature in WISPR data is sunlight scattered by dust in orbit around the Sun (F-corona); the secondary signal comes from sunlight scattered by electrons in the solar wind (K-corona). WISPR observes both the inner corona and the plasma in the vicinity of the spacecraft with a wide FoV. Due to the spacecraft's constantly changing distance to the Sun, the physical extent of WISPR's FoV changes through the orbit, and the resolution of the imaged features varies with distance to such features (Liewer et al. 2019). Looking out at PSP's orbital path ahead, WISPR connects the detailed but often uncontextualized *in situ* measurements to the larger context of the structures that contain them: a key science goal of the instrument. Tomography allows us to localize streamer features which WISPR images and compare them directly to measurements made by the *in situ* instrument suite.

3. METHOD

In this section we report on the technique by which we invert a sequence of synthetic images of the inner heliosphere for density structure in the vicinity of the spacecraft. We begin with the simplest approximation for the orbital geometry, with the goal of generalizing later. We later test the following methodology on a model dataset that we describe in Section 3.3.

We would like to reconstruct radial coronal structures proximal to PSP's orbit using synthetic WISPR image time series. To do so, we use *a priori* knowledge of these features to generate a family of curves that analytically describe their apparent motion in a FoV. Images of these analytic curves, viewed as vectors in a data space, form a partial basis of the data space formed by WISPR image sequences; this partial basis is, by construction, sufficient to represent the motion of stationary features through the FoV under simple linear translation of the spacecraft. We then create a 'T-Map' from our synthetic dataset, by extracting a particular transverse column from each image in the sequence and forming a composite image from the extracted columns. The T-Map shows how lateral angle (from the spacecraft) of features in the images varies over time, similar to the traditional 'J-Map' which Sheeley et al. (1999) first created with LASCO C2/C3 coronagraphs. A chronological ensemble of fixed position-angle strips from a set of images, a J-Map shows how solar elongation angle (the angle of a feature from the Sun from the observer's perspective) varies with time (Rouillard et al. 2020). Time-elongation or time-height maps have provided powerful means of tracking the evolution of coronal structures moving through the optically thin plasma (Rouillard et al. 2020). While the structures of interest to this research are not moving through the solar atmosphere but stationary over observation timescales, they nonetheless move through the FoV due to the spacecraft motion. As such, our T-Map captures this apparent motion and allows us to reconstruct coronal structure. Working with a single plane, we select a single transverse column from every image in order to build a lateral angle vs. time map.

With a T-Map and basis-vector curves in hand, we change the basis of the dataset from image coordinates to tomographic coordinates. Tomographic coordinates represent the space of all possible representable images, with the parameters used to create the trajectory maps. A 'tomogram' is an image created by enumerating the tomographic coordinates and calculating the dot product of the corresponding basis image for each location in the tomographic coordinate plane, with the actual T-Map data. Because the family of arctangent curves are not orthogonal in the linear algebra sense, simple tomograms are smeared even for cleanly separated modeled features, but they are adequate to centroid bright features near the modeled spacecraft. We will describe in the following section the simplest approximation of the

orbital geometry. Despite its simplicity, the fundamentals of the method apply to more generalized cases.

3.1. *The Linear Orbit Approximation*

Here we describe a "linear" Cartesian model of the apparent kinematics of stationary streamer strands near PSP's orbital track during an encounter period. It is the motion of spacecraft which produces apparent streamer motion in WISPR's field-of-view. This model approximates the spacecraft trajectory as a straight line (see Fig. 1 and Fig. 2), assuming the encounter period is sufficiently brief that curvature in the trajectory is negligible. The purpose of building a model for this problem is to reproduce the motion of streamers in WISPR's FoV to then compare to simulated or real data sets. We will then be able to change the basis from spacecraft coordinates to the tomographic coordinates in order to locate coronal striae in WISPR's FoV.

Returning to the spacecraft trajectory approximation of the model, we have elected to use the simplest approximation: a straight-line path. This approximation is valid on scales that are small compared to the orbital curvature. In other words, the sequence of images we use to perform tomographic reconstruction corresponds to a segment of PSP's orbit for which a straight-line path is a valid approximation. Furthermore, the perihelion speeds of $\sim$ a few hundred km/s render the radial features in WISPR's FoV effectively stationary; the timescale on which they evolve far exceeds that of the passing spacecraft.

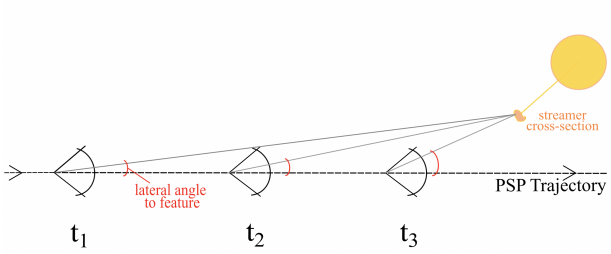

Figure 1: Cartoon depiction of Parker Solar Probe flying towards and past a solar wind feature whose cross-section appears above the horizontal trajectory; the spacecraft's viewing angle to the feature increases (in magnitude) as PSP approaches the feature.

As Fig. 1 shows, the spacecraft moves left to right, looking out at a streamer with cross-section indicated (not to scale). As the spacecraft approaches the feature, the magnitude of the viewing angle approaches 90° as the spacecraft approaches the feature. We can determine this angle using the appropriate trigonometric function: the arctangent function. Accordingly, we need two parameters- namely the ratio of two distances- to measure this angle. These two parameters characterize the distances parallel to the (linear) trajectory, the "along-track distance," and perpendicular to the trajectory, the "cross-track distance."

Fig. 2 illustrates the parameterization. As is evident from Fig. 1's pseudo-time-series, the parameter which changes in time is the along-track distance as the spacecraft flies along its linear track towards a streamer; meanwhile the cross-track distance remains fixed due to the quasi-stationary approximation for the streamer during the encounter. The time-evolving along-track distance thus results in a time-evolving viewing angle, which is the variable that which WISPR measures.

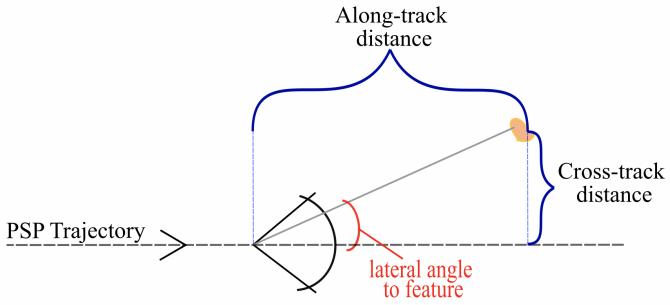

Figure 2: The locally lateral viewing angle to a feature in WISPR's field-of-view is directly determined by two parameters: the (diminishing) along-track distance to the feature and the (fixed) cross-track distance to the feature.

Next, we'll look at families of arctangent functions where one parameter is fixed and one parameter varies. These families of curves represent a small subset of all possible parameter pairs – all possible streamer locations in the proximity of PSP's track near perihelion.

3.2. *Modeling Apparent Kinematics with Arctangent Functions*

In order to invert for the locations of the features, we generate arctangent curves that model the motion of streamers as seen by WISPR. Specifically, we model the time evolution of the lateral angle to the feature in the WISPR FoV for all possible parameter pairs. By modeling WISPR data, either simulated or real, we can invert for the model parameters that best reproduce the data. In Section 3.4 we will show how we compare the analytic models to a simulated dataset, but for now we will look at some examples of the modeled curves; im-

ages of these curves partially span the data space that is a sequence of images, and we refer to these images as basis functions.

Fig. 3 shows two families of analytic feature paths (in the FoV) wherein one parameter is held fixed while the other is allowed to vary. Both plots illustrate how the viewing angle (from WISPR's point-of-view) to 20 different streamers changes as a function of time, as expressed in the unit of "timesteps" in order to easily scale the simulation to any dataset. For these plots, the speed of the spacecraft (along its linear trajectory) is set to 1 km/s, the speed of the streamers to 0 km/s, and the initial along-track distance of the streamer to an arbitrary number of "velocity-timesteps," in this case to the number of timesteps in the model dataset. The unit of distance – 'velocity-timesteps' – comes from the product of the spacecraft speed, which we assume to be constant during the encounter period, and the number of timesteps or images in the given dataset.

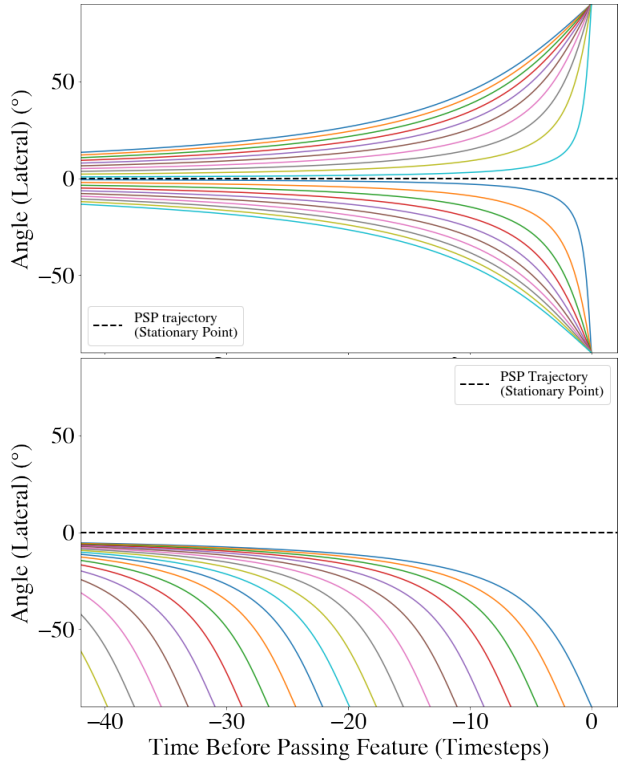

Figure 3: Two families of analytic feature paths used to create "basis images" for the tomographic inversion. The top panel models stria at constant along-track distance, while the bottom panel models stria at constant cross-track distance.

For both plots in Fig. 3, each curve denotes a different feature. The cross-track distance parameter varies between curves in the upper plot, akin to the spacecraft simultaneously passing 20 features at different perpendicular distances from the linear orbital track. Meanwhile, in the lower plot the along-track distance parameter varies between curves, which represents the spacecraft flying past one streamer at a time, all of which are located at the same perpendicular distance from the track.

Images of these curves, which match the characteristics of a WISPR T-Map, form a quasi-basis of the image data space, allowing a tomographic inversion.

3.3. *Pre-flight Visible-light Streamer Model*

In order to test how well the basis functions model the motion of coronal striae in WISPR's FoV, we applied our curves to a sequence of synthetic WISPR images built from a "ray-tracing software that computes white-light images of prescribed density models for any telescope with Thomson scattering effects included" (Liewer et al. 2019) (Thernisien et al. 2011). The model simulates WISPR's FoV as PSP flies through a finely structured stationary coronal streamer to which seven radial strands of circular cross section are constituent (Liewer et al. 2019). See Section 2. of Liewer et al. (2019) for further details about a very similar streamer model. The observing telescope in the simulation flies on a PSP orbit not corrected for solar rotation, with a perihelion of 11.6 $R_{\odot}$, and the streamer is fixed in heliographic latitude (Liewer et al. 2019). The FoV (48° by 95°) approximates the combined inner and outer FoVs of WISPR.

Fig. 4 illustrates a top-down view of the orbit segment used in the 11-h, 35-m perihelion pass simulation and the streamer strands through which the spacecraft flies.

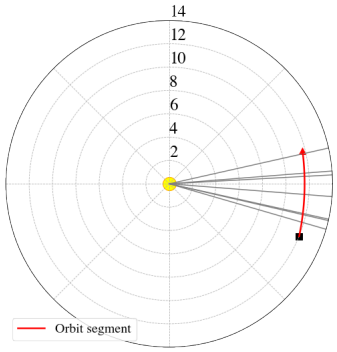

Figure 4: Aerial view of the simulated orbit (red curve) and the seven streamer strands (gray radial spokes) that PSP (black square) flies through during the encounter.

Figure 5 shows several images from this simulation. In the 3D data space (elongation, lateral angle, and time), Figure 3 illustrates cuts at a particular elongation, while the simulated images illustrate cuts at a particular time.

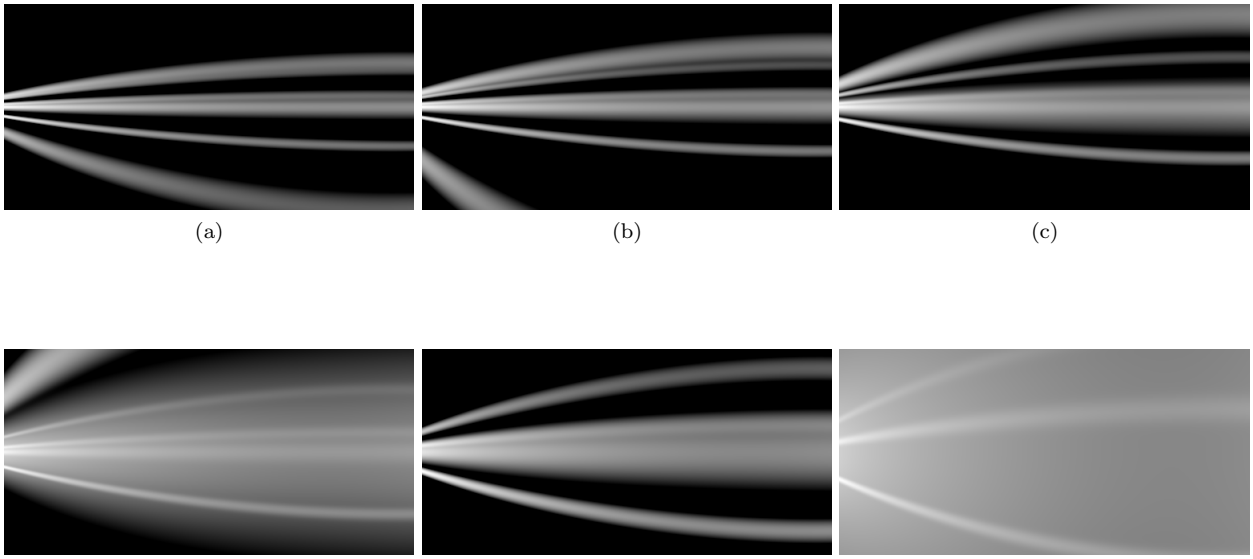

(a) (b) (c)

(d) (e) (f)

Figure 5: Six of 42 total images in the seven-strand streamer fly-through model with 90 min between each snapshot.

Akin to Figure 3 of Liewer et al. (2019), our Fig. 5 shows every sixth frame of the simulation – a cadence of 90 min in this subset. From the top left to the bottom right, these six images provide a crude illustration of the motion of the strands in the FoV. The streamers exit the top or the bottom of the FoV as PSP approaches the streamer, or remain stationary and expand to fill the FoV if PSP is on a collision course with a particular strand. The fourth and sixth panels show what WISPR sees when a strand is located along the spacecraft orbit: The feature washes over the FoV in these panels.

We can condense the image cube into a single image by selecting a single column of pixels from each image and stacking these columns in chronological order. From the 256x512 images, we chose the column of pixels (column 400) at which the features appeared horizontal (i.e. not expanding) in the image plane. Every column maps to a specific time during the simulation, and thus our 'T-Map' shows how the lateral angle to the features evolves in time. Appearing in Fig. 6, the T-Map derived from the model flythrough captures the temporal evolution of strand motion in the FoV.

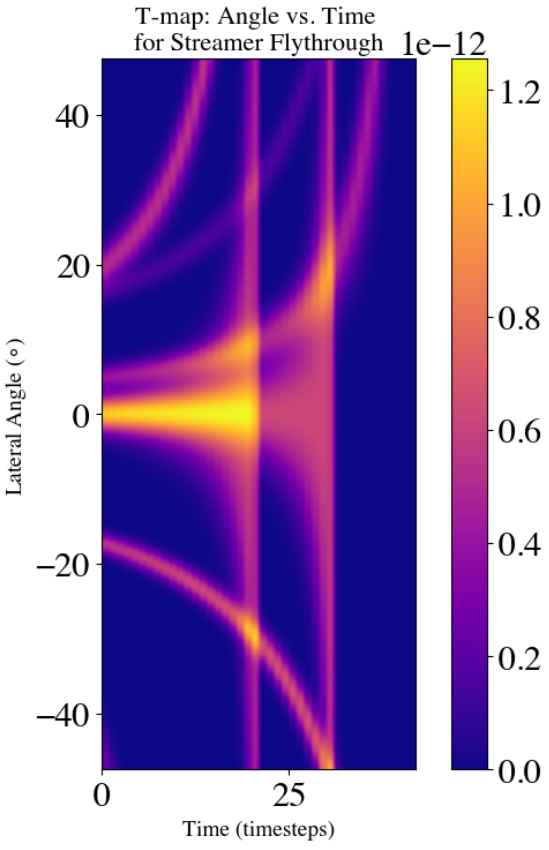

Figure 6: The T-Map produced for the seven-strand streamer flythrough.

This 'trumpet diagram' gives qualitative insight into the streamer strand parameters: how far along the orbital path and how far from the orbital path each of the strands was during the simulated observation. Curves that diverge out of the top (bottom) of the image (FoV) indicate strands which PSP flew below (above). On the other hand, curves that span the entire angular extent correspond to strands positioned directly on PSP's trajectory; PSP flies directly through them. The curves that exit the FoV at earlier times indicate closer placement to PSP's initial position, along the orbital path. Additionally, curves with steeper gradation indicate features of closer proximity to the spacecraft than those with a gentler slope.

We next overplot analytic arctangent curves on our T-Map to show how this analytic form captures the general geometry of the curves in our T-Map. Later on, we will discuss the sensitivity with which we need to capture the geometric form of the curves in the T-Map in order to produce accurate reconstructions.

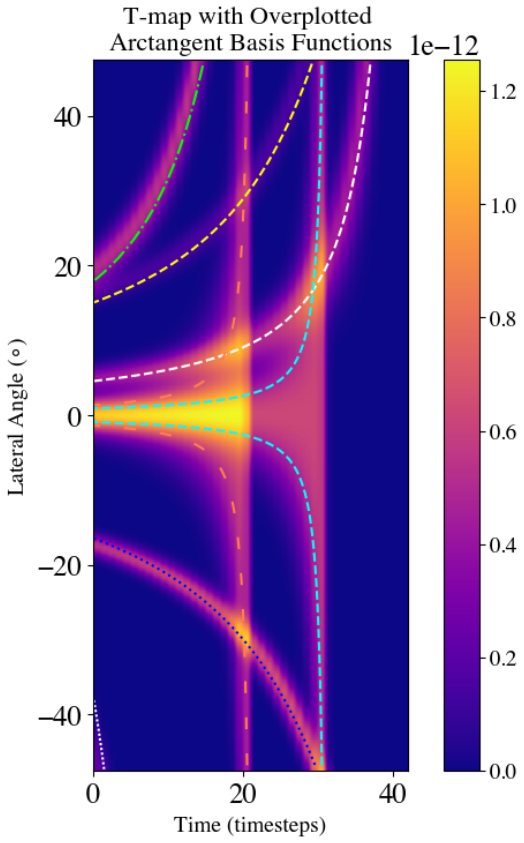

Figure 7: We can see that our analytic feature paths can effectively track the curves from the T-Map, showing that the ansatz (initial guess) of arctangent functions in this linear orbit approximation was a reasonable choice.

As Fig. 7 shows, we can produce shapes that track the curves in the T-Map. Next, we will explain how we change the basis of our dataset from temporal variation of lateral angle back to our original parameters: along-track and cross-track distance. This simple change of basis yields a tomogram containing the positions of the features with respect to the spacecraft track.

3.4. *Changing the Basis to Parameter Space*

Our goal is to change the basis from the time variation of lateral angle – 'image coordinates' – to the along-track and cross-track distances – 'tomographic coordinates.' However, the non-orthogonality of our (partial) basis means that we cannot uniquely determine the two parameters which yielded the observed angular time evolution. However, this inversion theoretically still allows us to constrain the positions of the coronal striae.

The first step in changing the basis is to produce an arctangent basis element for each unique pair of parameter values (within a parameter subspace selected *a priori*). We allow the along-track parameter to go from 0 to the number of timesteps in the simulation (or the number of images in the sequence), and we allow the cross-track parameter to span distances $\leq$20 velocity-timesteps from the linear spacecraft track. These cross-track distances encompass all strands that would appear in WISPR's FoV.

Having produced normalized 'image curves' for all parameter pairs in this subspace, we then take a simple dot product of each image curve with the T-Map. In doing so, we measure the correlation between a given curve and the T-Map. Note that because our basis functions are not orthogonal, the dot product can take on continuous values between 0 and 1. We assign the value of each dot product operation to a pixel location on an output image with coordinates corresponding to the parameter pair that characterized the curve in question. In other words, the so-called 'tomogram' output image has dimensions of along-track (x-direction) and cross-track distance (y-direction), and every point on this image corresponds to a parameter pair assigned to an image curve that we dotted into the T-Map. In the following section, we analyze our first-cut results and compare the reconstructed plane to the simulation's ground-truth locations of the streamer footpoints.

4. RESULTS AND VALIDATION

In this section, we show the results of our inversion: the tomogram. Recall that our goal was to reconstruct coronal density structure in the proximity of PSP. The tomogram (Fig. 8) indicates the positions of the streamer strands along the track (in the direction of the Probe's linear motion) and from the track (in the direction perpendicular to the straight-line path). Each region of enhanced signal corresponds to a streamer strand on the T-Map and indicates where the strand intersected with a plane along the trajectory and perpendicular to it. Each centroid indicates the parameter pair that best describes a stria in the simulation.

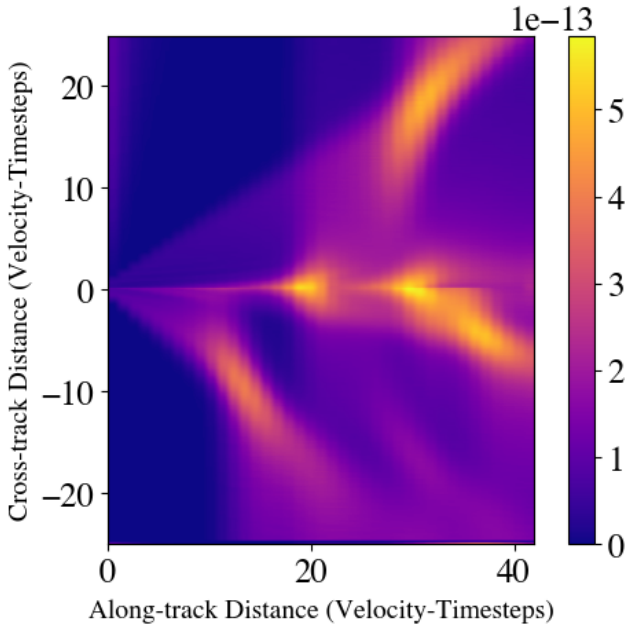

Figure 8: The tomogram for the seven-strand model of a coronal streamer. Bright extended regions indicate positions of the seven streamers during the PSP simulated flythrough in terms of the two parameters.

We see that rather than discrete points which would precisely determine the locations of the streamers, the tomogram instead displays diffuse areas of higher signal, which span ranges of values in both parameters. This effect is explained by the non-orthogonality in our arctangent basis. When dotted with the T-Map, multiple parameter pair combinations will result in nonzero inner products, which thereby produces extended regions of nonzero signal. There is not, therefore, a singular position for each streamer but a spread of values that yield the observed angular evolution. Furthermore, features with larger cross-track distances result in more diffuse regions, and thus less accurate position inversions, on the tomogram. We will discuss the challenges of non-orthogonality and the nuanced geometry of the basis functions further in Section 5.

Before we do so, however, we need to compare the solutions of the inversion to the projected locations of

the ground-truth footpoint locations out to the 'sidewalk strip' coplanar with our tomogram.

To create the simulated flythrough, Thernisien et al. (2011) assigned angular locations to the streamer strand, i.e. where the strands are rooted in the photosphere. Knowing these footpoint latitudes and longitudes, we applied a Gnomonic projection to map these locations out to the plane along the 'sidewalk strip' that runs both parallel and perpendicular to the track, with the perpendicular direction running along the heliographic North-South line and the parallel direction coincident with the straight line-approximated orbit.

The following figure illustrates how the strands are projected out to a plane located at the perihelion distance for the simulated orbit. Fig. 10 (b) then shows two projections: one which projects the strands out to a spherical surface whose radius equals the perihelion distance and one which project the strands out to a plane situated at the perihelion distance (i.e. a Gnomonic projection). Fig. 9 helps elucidate how a point's location is mapped to a plane tangent to a sphere.

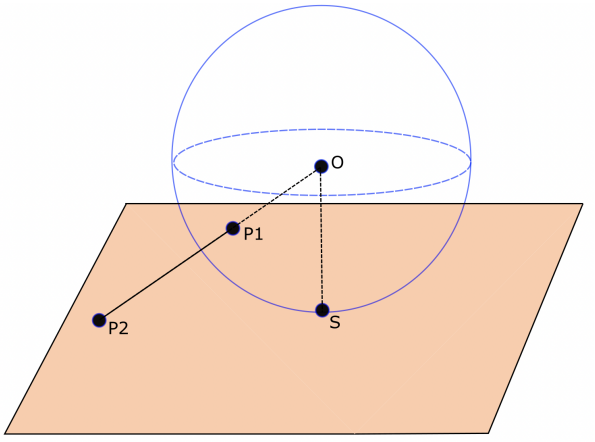

Figure 9: Diagram of the Gnomonic projection: mapping a point P1 on a sphere out to a plane, which is tangent to the sphere at point S. Note that P1 need not lie on the sphere defining the projection; the only requirement for P1 is that it is a point on *a* sphere.

Referring back to our tomogram (Fig. 10a) whose centroids are highlighted (by approximation), we can see that the constellation of bright spots do not match the points as determined by the Gnomonic projection out to the perihelion plane (Fig. 10b). Namely, the regions corresponding to features with larger cross-track distances are more displaced in the along-track direction than the features perpendicularly closer to the orbital path.

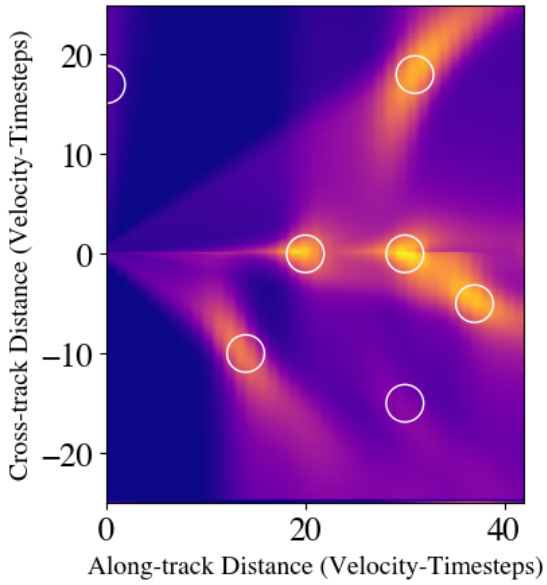

(a) This tomogram highlights each striae's intersection with the reconstructed plane as determined by our tomographic method.

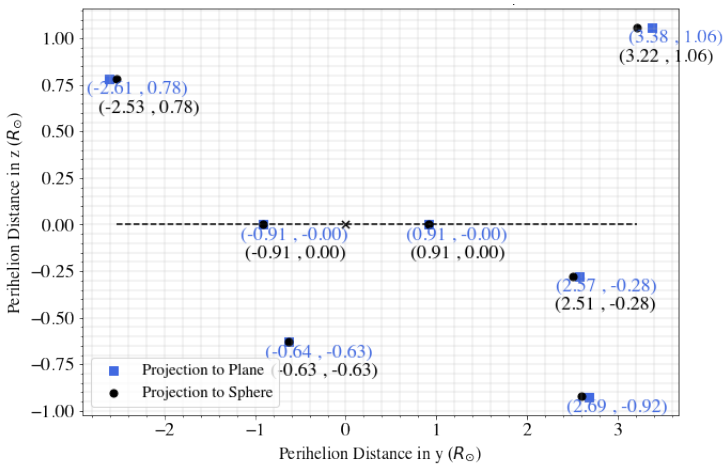

(b) This plot indicates the locations of streamer footpoints on a plane situated at perihelion and on a sphere with a radius equal to the perihelion distance of the simulation.

Figure 10: Here we show the two figures adjacent to one another to allow the reader to more easily compare the two constellations of points to each other. Highlighted regions in (a) may assist the reader in comparing tomogram centroids to the blue squares in (b), which are the Gnomonic projections of the striae.

5. DISCUSSION

As we presented in the previous section, our tomographic inversion failed to reproduce the correct locations of the streamer strands. We tested the results of the tomography by mapping the angular locations of the streamer footpoints from the simulation out to

a plane located at the perihelion distance of the simulation. This plane is coplanar with the reconstructed plane, i.e. the tomogram. We think that a nonlinear combination of different effects resulted in our results failing to reproduce the known footpoint locations. The non-orthogonality of the basis functions, the fixed viewing plane for the linear orbit approximation, and the projection used for the simulated flythrough could be interacting in such a way that offsets the inverted striae positions on the tomogram from the true positions on that plane.

Regarding the partial basis with which we are reconstructing the nearby corona, the issue of non-orthogonality presents myriad issues. The similarity of neighboring basis elements results in a large number of parameter pairs all yielding similar dot product values. Consequently, we see continuous, extended regions of nonzero value on our tomogram, i.e. non-localized position inversions. Coming back to the relationship between the cross-track distance and the offset of the inverted position from known position, we see that the error increases with the magnitude of cross-track distance. Again, the non-orthogonality issue plays a substantial role: The basis element of a feature with a large cross-track distance has a less-steep vertical component than one with a small cross-track distance. As such, this element is less differentiable from its neighboring elements. Features with large cross-track distances, therefore, suffer larger uncertainties in reconstructed positions than those closer to the orbital track in the perpendicular direction. We will work to develop the error dependence on cross-track distance more rigorously when we move into working with WISPR data.

Furthermore, for such a large family of basis vectors, there lie substantial challenges in building an orthogonal basis. Gram-Schmidt orthogonalization is a technique which orthogonalizes a non-orthogonal basis by removing the projection (i.e. parallel component) of one vector onto another vector. This large family of high-dimensional basis vectors makes direct orthogonalization prohibitively difficult via direct inversion, though sparse-matrix methods may prove useful in future work.

We can also explore the question of which plane our orbital model captures and thus which tomographic plane we thereby reconstruct. The following figure shows how the locations of the streamer intersections vary with different tomographic planes that all originate from the spacecraft. This example illustrates how the particular orbit approximation and the determination of direction of motion from the dataset can confuse the location at which the inversion determines feature positions. While the linear orbit approximation selects a singular plane with which the streamers intersect, the spacecraft actually moves along an elliptical orbit, and thus the plane of streamer intersection changes continuously. Therefore, our simple orbit path approximation might be reconstructing a plane that does not correspond to the direction of motion.

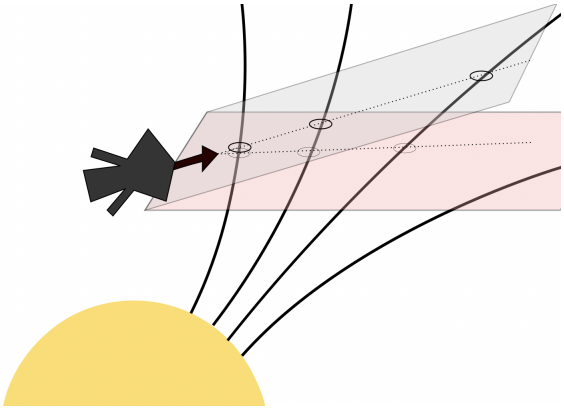

Figure 11: The dihedral problem: Coronal striae intersect two planes extending from PSP. The gray-colored plane corresponds to the spacecraft's direction of motion (denoted with a black arrow) at an instant in time – the correct plane for translational tomography.

Our next step will be to reformulate the geometry of the problem in order to more accurately model the motion of the streamer strands in WISPR's FoV. In this future geometric approximation, we will take PSP's orbit to be circular, constrained to the orbit plane, and use three-dimensional (3D) spherical geometry to relate the time-dependent spacecraft location to a fixed point on a stria.

Fig. 12 (Fig. 2 from Liewer et al. (2022, submitted)) illustrates the geometry that we adopt in this three-dimensional spherical framework. As we can see, five angles uniquely define the locations of the spacecraft and of the streamer: the difference in orbital anomalies (in-plane angles) of the streamer and spacecraft is defined by $\phi_2 - \phi_1$, the in-plane viewing angle to the feature is γ, the out-of-plane viewing angle to the feature is β, and the quasi-latitude of the streamer is δ_2. This last angle is the feature's angle out of the orbit plane, which is close but not equivalent to the solar equatorial plane. We can think of the angles γ and β as our spacecraft coordinates, and ϕ_2 and δ_2 as our feature coordinates. We seek to invert for the feature coordinates ϕ_2 and δ_2 by modeling how the angle β changes as a function of ϕ_1, for values of γ that correspond to the angular extent of WISPR's FoV.

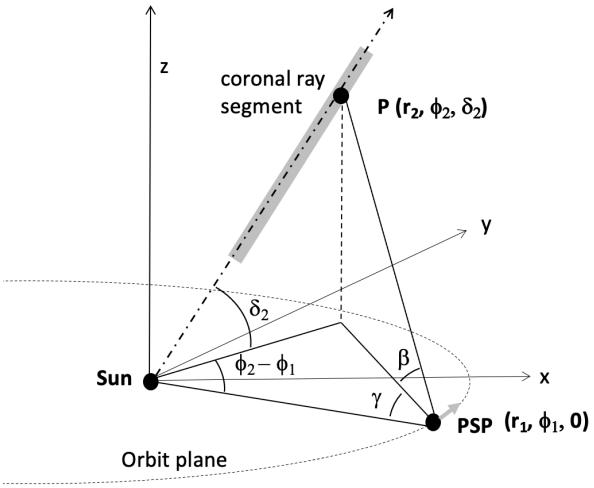

Figure 12: Spherical geometry for PSP-WISPR and coronal helmet streamers. Fig. 2 from Liewer et al. (2022, submitted).

In closed form, we can construct a new set of functions to describe how the out-of-plane viewing angle, β, varies as the spacecraft moves along its orbit and looks out at a stationary radial feature. The next paper in this sequence on translational tomography for WISPR will explore the geometry of the new set of basis functions and how it and its resulting tomograms compare to those of the linear orbit approximation.

6. CONCLUSION

In this paper, we have described a simplified geometric framework for the spacecraft motion (i.e. a linear spacecraft orbit) and for parameterizing the locations of radial features' cross-sections. In describing the cross-sectional locations with along-track and cross-track distance parameters, we analytically modeled the apparent motion of striae in WISPR's FoV. We then constructed a family of basis vectors, or image curves, corresponding to the parameter subspace appropriate to the problem: features with along-track distances during the observation window and cross-track distances with absolute value less than $\sim$25 velocity-timesteps.

Using the simulated flythrough dataset in order to test our method, we transformed the sequence of 42 images of seven streamer strands in the corona into a single image called a T-Map. We created this composite image by extracting the 400th column from each image and stacking these columns in chronological order. The T-Map therefore tells us how the streamers temporally evolve over flythrough: when they leave the FoV and how close they were to the spacecraft track – in the perpendicular direction. We then measured how well the image curves correlated with the curves in the T-Map (i.e. changed the basis) by taking the dot product of each basis element (x_i, y_j) with the T-Map and populating a pixel (x_i, y_j) on the tomogram with that dot product value. The higher the signal in a region of pixels on the tomogram thus indicates a better alignment between the parameter pair of that basis element (x_i, y_j) and a particular curve on the T-Map.

Our tomogram gave us insight into where the synthetic dataset's streamers intersected with the sidewalk strip along PSP's orbital track. However, in comparing our inversion to the projected ground-truth streamer footpoint locations, we found that our results did not match the known positions. We explored possible reasons for why the linear orbital approximation, a highly-simplified geometric model for the spacecraft motion near perihelion, failed to reproduce the correct positions on the plane. We also introduced the spherical geometric framework that will better describe the spacecraft motion and better parameterize streamer positions as seen by the WISPR instrument.

Despite the limits of this most simple inversion, we have shown that the method is capable of extracting positions of radial, stationary, faint features that appear in the (synthetic) WISPR FoV. Despite the small line-of-sight integration and contrast as a result of WISPR's viewing angles perpendicular to these striated structures, rather than parallel to them, we have leveraged the time-integration of the dataset through a sequences of images near perihelion to deduce where these structures were situated during the simulated solar encounter. The general method nonetheless shows promise to accurately reconstruct radial density structures in the vicinity of PSP, despite the results of the simple analytic model we explored in this first attempt. This work suggests that, with improvements to the geometry used to construct analytic models; further exploration of the synthetic flythrough; and changes to the ways we reflect the spacecraft direction of motion in our reconstruction, we will be able to reconstruct the locally lateral plane along PSP's trajectory near perihelion.

Only when we are able to reproduce the ground-truth locations of the streamers in the model flythrough can we then apply this method to the actual WISPR data. Accurate inversions of faint, stationary structures that appear in WISPR's FoV near perihelion would enable us create detailed maps of coronal density structure local to PSP, thereby providing context for other instruments on the PSP payload as well as ground-based telescopes looking in the vicinity of PSP during solar encounters. As PSP successively dives closer to the Sun, this method will grow in utility.

7. ACKNOWLEDGMENTS

I am grateful to my advisor, Craig DeForest, for his support throughout my first two years in graduate school. I am also grateful for the support from my collaborators who have likewise helped me get my footing in heliophysics and graduate school alike. We thank the PSP team for bringing to life a beautiful new mission as well as the WISPR team for developing the WISPR instrument to enable novel science opportunities and for cultivating a strong and collaborative scientific community. This material is based upon work supported by the National Science Foundation Graduate Research Fellowship under Grant DGE 1650115. We thank the National Science Foundation for its support of basic science research.

REFERENCES

Altschuler, M. 1979

Aschwanden, M. 2006, Physics of the solar corona: an introduction with problems and solutions (Springer Science & Business Media)

Brueckner, G., Howard, R., Koomen, M., et al. 1995, in The SOHO mission (Springer), 357–402

Decraemer, B., Zhukov, A. N., & Doorsselaere, T. V. 2019, The Astrophysical Journal, 883, 152, doi: 10.3847/1538-4357/ab3b58

DeForest, C. E., Howard, T. A., & Tappin, S. J. 2011, ApJ, 738, 103, doi: 10.1088/0004-637X/738/1/103

Eyles, C., Simnett, G., Cooke, M., et al. 2003, Solar physics, 217, 319

Fox, N., Velli, M., Bale, S., et al. 2016, Space Science Reviews, 204, 7

Frazin, R. A. 2000, The Astrophysical Journal, 530, 1026

Frazin, R. A., & Janzen, P. 2002, The Astrophysical Journal, 570, 408

Golub, L., & Pasachoff, J. M. 2010, The solar corona (Cambridge University Press)

Howard, R. A., Moses, J., Vourlidas, A., et al. 2008, Space Science Reviews, 136, 67

Jackson, B., Hick, P., Buffington, A., et al. 2011, Journal of Atmospheric and Solar-Terrestrial Physics, 73, 1214

Koutchmy, S. 1994, Advances in Space Research, 14, 29, doi: https://doi.org/10.1016/0273-1177(94)90156-2

Liewer, P., Vourlidas, A., Thernisien, A., et al. 2019, Solar Physics, 294, 1

Liewer, P., Hall, J., De Jong, M., et al. 2001, Journal of Geophysical Research: Space Physics, 106, 15903

Menke, W. 2018, Geophysical data analysis: Discrete inverse theory (Academic press)

Panasyuk, A. V. 1999, Journal of Geophysical Research: Space Physics, 104, 9721

Rouillard, A. P., Kouloumvakos, A., Vourlidas, A., et al. 2020, The Astrophysical Journal Supplement Series, 246, 37

Sasso, Pinto, R. F., Andretta, V., et al. 2019, A&A, 627, A9, doi: 10.1051/0004-6361/201834125

Sheeley, N. R., Walters, J. H., Wang, Y. M., & Howard, R. A. 1999, J. Geophys. Res., 104, 24739, doi: 10.1029/1999JA900308

Thernisien, A., Vourlidas, A., & Howard, R. 2011, Journal of Atmospheric and Solar-Terrestrial Physics, 73, 1156

Vásquez, A. M., Frazin, R. A., Vourlidas, A., et al. 2019, Solar Physics, 294, 1

Vourlidas, A., Howard, R. A., Plunkett, S. P., et al. 2016, Space Science Reviews, 204, 83